Primljen / Received: 16.6.2025.
Ispravljen / Corrected: 17.9.2025.
Prihvaćen / Accepted: 30.10.2025.
Dostupno online / Available online: 10.2.2026.

Flexural capacity prediction of partially encased composite beams using machine learning

Authors:

[1,2]Prof. **Hongxin Liu**
Liuhx@aisa.com.cn

[3]**Ping Yang**, MCE
316376606@qq.com

[1,2]Prof. **Yaming Li**
Liym@aisa.com.cn

[1,2]Prof. **Shuizhong Jia**
Jiasz@aisa.com.cn

[4]**Xiaomeng Xie**, PhD. CE
xiexiaomeng2024@163.com
Corresponding author

[1] Shanghai Institute of Architectural Design and Research, d.o.o., China
[2] Shanghai Spatial Structure Engineering Research Center, China
[3] Government Construction Project Center of Kangbashi District, China
[4] Shanghai Jieyi Construction Technology Co., Ltd., China

Original research paper

Hongxin Liu, Ping Yang, Yaming Li, Shuizhong Jia, Xiaomeng Xie

Flexural capacity prediction of partially encased composite beams using machine learning

To address traditional limitations, this study investigated the flexural performance of large-section PEC beams with varied web openings using experiments and machine learning (ML). Four-point bending tests on specimens with different sections and openings demonstrated excellent ductility (coefficient >4.0), although openings slightly reduced yield strength without significantly affecting overall performance. A database of 15 variables was used to train and validate four ML models (RF, CatBoost, KNN, LightGBM). The RF model achieved the highest accuracy (~2.6% MAE). Shapley analysis improved interpretability by identifying key parameters. Integrating explainable ML substantially enhances the prediction accuracy and interpretability of PEC flexural capacity, offering a promising approach for intelligent structural design and assessment.

Key words:
PEC beams, failure mode, flexural capacity, ductility, machine learning

Izvorni znanstveni rad

Hongxin Liu, Ping Yang, Yaming Li, Shuizhong Jia, Xiaomeng Xie

Predviđanje savojne nosivosti djelomično obloženih kompozitnih greda pomoću strojnog učenja

Radi prevladavanja ograničenja tradicionalnih metoda u ovome istraživanju ispitana je savojna nosivost djelomično obavijenih kompozitnih (PEC) greda velikog presjeka s različitim otvorima u hrptu pomoću eksperimentalnih ispitivanja i strojnog učenja (ML). Ispitivanja savijanjem u četirima točkama na uzorcima različitih presjeka i tipova otvora pokazala su vrlo dobru duktilnost (koeficijenti > 4,0), pri čemu su otvori u hrptu blago smanjili granicu tečenja, ali bez znatnijega gubitka nosivosti. Baza podataka s 15 parametara korištena je za treniranje i validaciju četiriju modela ML (RF, CatBoost, KNN, LightGBM). Model Random Forest pokazao je najveću točnost (≈ 2,6 % MAE). Primjenom analize Shapley unaprijeđena je interpretabilnost modela te su identificirani ključni parametri. Integracija objašnjivoga strojnog učenja znatno poboljšava točnost i razumljivost predviđanja savojne nosivosti PEC greda, nudeći učinkovit pristup za inteligentno projektiranje i procjenu konstrukcija.

Ključne riječi:
PEC grede, oblik otkazivanja, savojna nosivost, duktilnost, strojno učenje

1. Introduction

Steel-concrete composite beams are a type of composite structure that effectively combine the excellent compressive strength of concrete with the high tensile strength and ductility of steel [1-5]. Partially encased composite (PEC) components are formed by placing shear connectors within the flanges of structural steel sections and casting concrete around them [6-9]. During prefabrication, PEC components require only side formwork, thereby simplifying formwork requirements. The presence of concrete within the flanges effectively reduces the risk of both overall and local buckling, playing a crucial role in enhancing the load-bearing capacity of the structure [10]. Compared with traditional steel components, PEC beams exhibit excellent fire resistance [11-13], and significantly improved bending and shear performance [14-15].

To date, numerous researchers have investigated the mechanical properties and applications of PEC beams. Nakamura et al. [16] found that the flexural and shear load-bearing capacities of PEC beams are 2.08 and 2.98 times greater, respectively, than those of traditional I-section steel beams. He et al. [17, 18] demonstrated through experiments and numerical simulations that PEC beams with corrugated steel webs possess higher shear strength and fracture modulus, and they proposed a calculation method for their shear load-bearing capacity. Nardin et al. [19] examined the effects of different construction methods on the flexural performance of PEC beams, with experimental results indicating that the presence of bottom bolts improves the fracture modulus. Kindmann et al. [20] conducted bending tests on 12 PEC beams with different cross-section types, showing that concrete within the flanges enhances both the flexural load-bearing capacity and stiffness. The use of new concrete materials with higher tensile properties has further improved the flexural performance of steel-concrete composite beams [21-23]. Hao et al. [24] carried out shear tests on PEC-UHPC composite beams, revealing their superior shear performance. Zhao et al. [25] proposed two new types of honeycomb PEC beams and studied the effects of web openings, compressed steel flanges, and filled concrete on mechanical performance; however, comprehensive and systematic studies remain limited. Compared with traditional steel beams, PEC beams exhibit improved load-bearing capacity and ductility. However, calculation methods for the flexural bearing capacity of different types of PEC beams have not yet been fully defined. Consequently, more robust analytical approaches are required to investigate the flexural performance of PEC beams and to address the limitations of conventional methods. Machine learning offers considerable advantages in handling large datasets and capturing complex nonlinear relationships, and it can enhance prediction accuracy by filtering out variables that have minimal influence on the output. In recent years, machine learning has seen increasingly widespread application in civil engineering, including construction cost estimation, concrete splitting tensile strength, shear performance of beams, the seismic behaviour of reinforced concrete columns [30], the shear strength of concrete joints, and structural seismic response [26-32], thereby demonstrating its notable adaptability. However, despite its growing use in various civil engineering applications, no systematic study has yet applied machine learning to predict the flexural capacity of PEC beams.

2. Methodology

To provide a clear overview of the research process, the overall methodology adopted in this study is summarised in Figure 1. The workflow comprises the following steps:

1. **Database development:** A dataset of 152 PEC beams was compiled from the literature and experimental programmes, incorporating 15 key geometric, material, and structural parameters.
2. **Feature evaluation and selection:** Correlation analysis and feature-importance ranking were conducted to identify the most relevant input variables, thereby ensuring model robustness and avoiding redundancy.
3. **Model training and optimisation:** Four machine learning algorithms (KNN, LightGBM, CatBoost, and RF) were developed and tuned through cross-validation and Bayesian optimisation to improve predictive accuracy. The algorithms include: a) K-Nearest Neighbours (KNN) [33], a straightforward and efficient supervised learning algorithm known for strong performance in both regression and classification tasks; b) Light Gradient Boosting Machine (LightGBM) [34], a gradient boosting framework optimised for fast training and low memory consumption, well suited to large-scale datasets; c) CatBoost [35], a categorical boosting algorithm designed to minimise bias when handling categorical features during gradient boosting; and d) Random Forest (RF) [36], an ensemble learning method that combines multiple decision trees to reduce variance and enhance generalisation.
4. **Model interpretation:** The SHAP method was applied to interpret the predictive outcomes and identify the most influential structural parameters governing flexural capacity.
5. **Experimental validation:** Four-point bending tests on PEC beams with different web opening configurations were conducted to verify the practical applicability of the proposed models.
6. **Comparison with traditional formulas:** Predictions from the machine learning models were benchmarked against conventional plastic theory formulas to assess accuracy and conservativeness.
7. **Verification and conclusions:** The predictive performance of all methods was compared, the most reliable model was identified, and the implications for engineering practice were discussed.

This structured framework ensures methodological transparency and demonstrates how each step contributes directly to accurate and interpretable prediction of PEC beam flexural capacity.

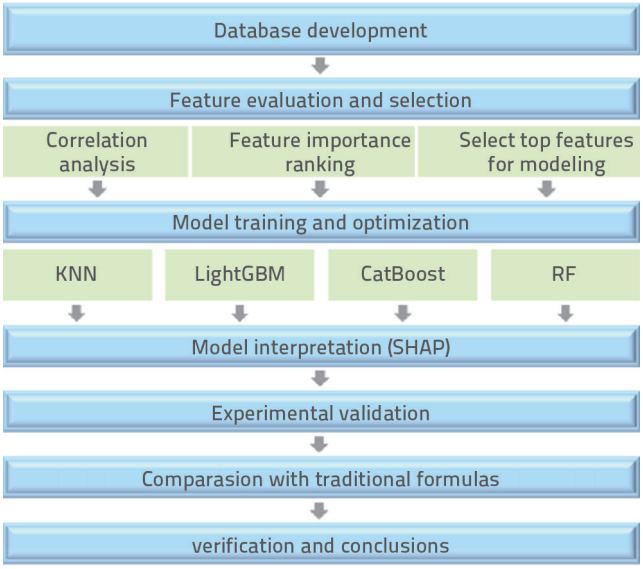

Figure 1. Overall workflow diagram

3. Prediction method for flexural capacity based on machine learning

With the growing integration of artificial intelligence into civil engineering, machine learning algorithms have become powerful tools for rapidly replicating experimental findings and accurately predicting structural behaviour. This study aims to develop a machine learning-based prediction model for the flexural capacity of PEC beams and to validate its accuracy using experimental data.

3.1. Display and evaluation of the PEC beam flexural bearing capacity database

To enhance the predictive performance of the proposed model, an extensive dataset was compiled using experimental results from researchers across multiple countries, comprising 152 prestressed PEC beams reported in references [37-53]. The output parameter was defined as the flexural capacity *y*, and fifteen key input variables influencing the flexural performance of partially encased composite (PEC) beams were selected, as detailed in Table 1.

Figure 2 illustrates the distribution of the 15 input variables in relation to the flexural capacity y. Linear regression analysis revealed that variable x_2 exhibited the strongest correlation with *y*, achieving a coefficient of determination R^2 of 0.7504. This was followed by x_5, x_6, and x_{14}, with respective R^2 values of 0.7263, 0.7272, and 0.6140. In contrast, the remaining variables showed relatively weak correlations with flexural capacity, with the highest R^2 among them being only 0.3970.

High correlations among input variables can lead to model overfitting and reduced interpretability, ultimately undermining prediction reliability. To evaluate the interrelationships between input features, Spearman correlation analysis was conducted. Unlike the traditional Pearson coefficient, which measures only linear associations, the Spearman correlation captures both linear and nonlinear dependencies, providing a more comprehensive assessment. The correlation matrix is presented in Figure 3. The output parameter (*y*) was also included in the matrix for visualisation purposes, allowing readers to directly observe the correlation between each input and the flexural

Table 1. Detailed interpretation of the 15 variables

Variable	Unit	Description
x_1	mm	Beam width
x_2	mm	Beam height
x_3	mm	Flange thickness
x_4	mm	Web thickness
x_5	mm	Upper web height
x_6	mm	Lower web height
x_7	mm^2	Reinforcement area
x_8	/	Reinforcement ratio
x_9	MPa	Reinforcement yield strength
x_{10}	MPa	Flange yield strength
x_{11}	MPa	Web yield strength
x_{12}	MPa	Concrete compression strength
x_{13}	/	Proportion of concrete area
x_{14}	/	Proportion of steel area
x_{15}	mm	Shear span length
y	kNm	Flexural capacity

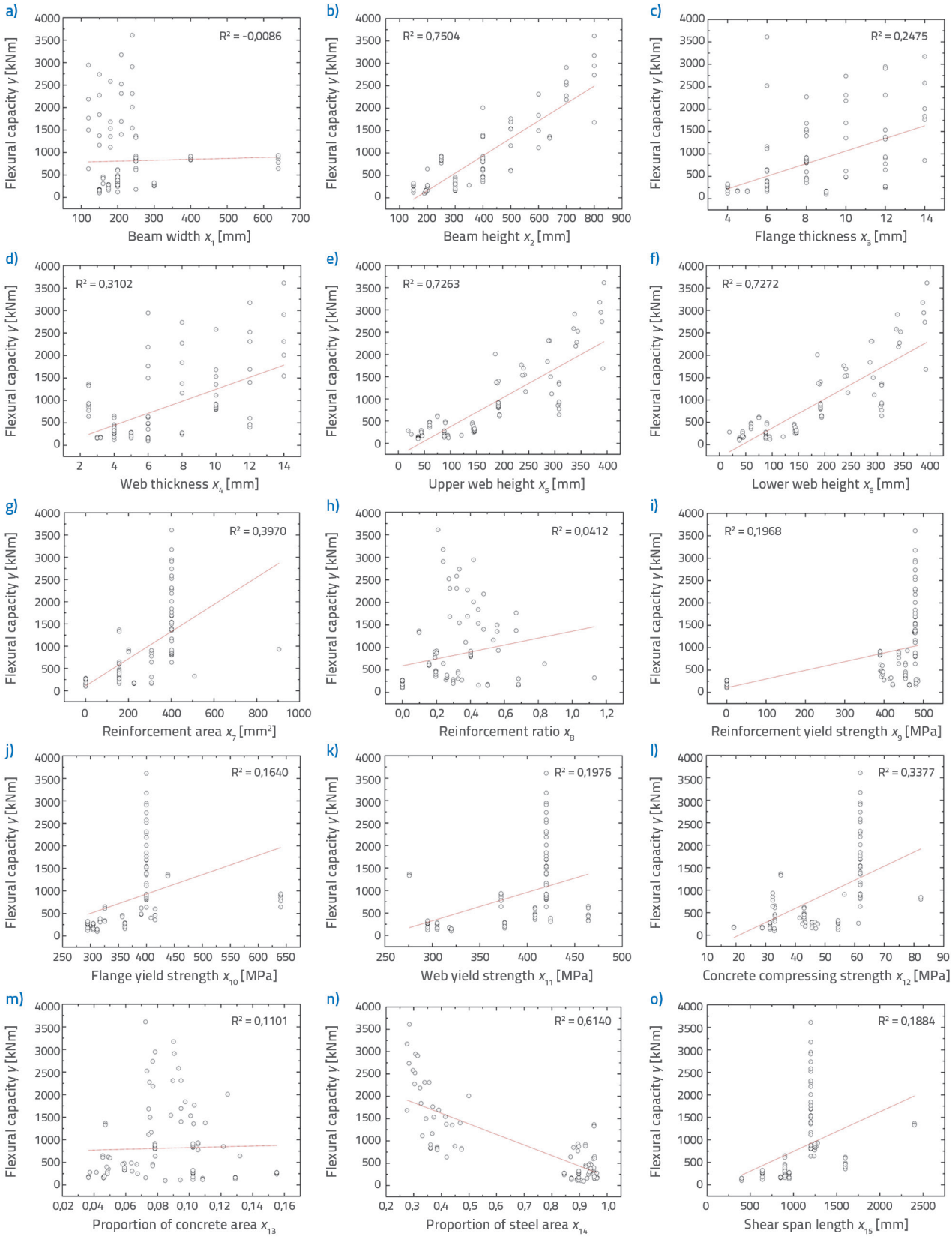

Figure 2. Dataset presentation: a) Beam width x_1; b) Beam height x_2; c) Flange thickness x_3; d) Web thickness x_4; e) Upper web height x_5; f) Lower web height x_6; g) Reinforcement area x_7; h) Reinforcement ratio x_8; i) Reinforcement yield strength x_9; j) Flange yield strength x_{10}; k) Web yield strength x_{11}; l) Concrete compression strength x_{12}; m) Proportion of concrete area x_{13}; n) Proportion of steel area x14; o) Shear span length x_{15}

capacity; however, *y* was not considered in the collinearity assessment. The results revealed strong correlations (coefficient > 0.70) between several variable pairs, including x_1 and x_{10}, x_2 and x_5, x_2 and x_6, x_5 and x_6, x_7 and x_8, and x_7 and x_9.

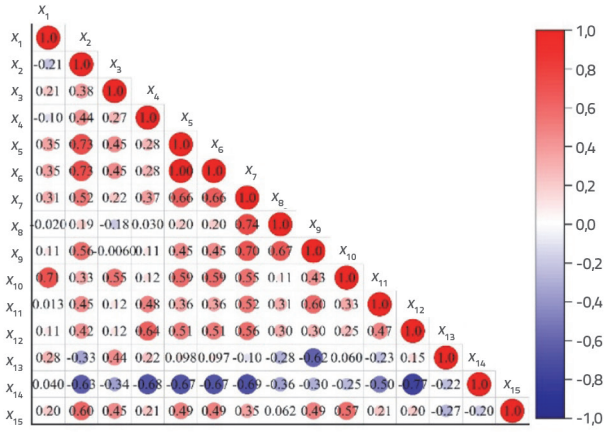

Figure 3. Spearman correlation coefficient matrix for input and output parameters

It should be noted that the inclusion of *y* is solely for visualisation, intended to illustrate the degree of correlation between each input feature and the target output. Collinearity analysis was performed exclusively among the input variables, with pairs exhibiting coefficients greater than 0.70 considered strongly correlated.

Figure 4.a presents the variable-importance scores obtained from the four predictive models (KNN, LightGBM, CatBoost, RF), each using its respective importance-calculation procedure:

- KNN - permutation importance with 5-fold cross-validation (R^2 as the metric, n_repeats = 30, random_state = 42), with the best hyperparameters selected through a manual search over n_neighbors ∈ {3,...,15} and weights ∈ {uniform, distance}.
- LightGBM - gain-based importance from the tuned LGBMRegressor (hyperparameters optimised via Bayesian search within num_leaves ∈ [31, 127], learning_rate ∈ [0.05, 0.25], n_estimators ∈ [200, 800], with others at default).
- CatBoost - PredictionValuesChange importance from the tuned model (iterations ∈ [300, 1000], depth ∈ [4, 8], learning_rate ∈ [0.05, 0.25], random_state = 42), with SHAP applied as a robustness check.
- Random Forest - impurity-based importance (MDI) from the tuned RF (n_estimators = 500, max_features = "sqrt", min_samples_leaf = 2, random_state = 42, others at default), cross-checked using permutation importance (n_repeats = 30).

All importance scores were min-max normalised and subsequently summed across methods. The stacked bars in Figure 4.b display the combined importance score (total height) together with the relative contributions from each method (colour segments).

It should be noted that KNN - permutation importance with 5-fold CV (R^2 metric, n_repeats = 30, random_state = 42); LightGBM - gain-based importance from the tuned LGBMRegressor; CatBoost - Prediction Values Change importance from the tuned model (with a SHAP check); RF - impurity-based importance (MDI) from the tuned model, cross-checked using permutation importance. All importance scores were min-max normalised and summed. The total bar height represents the combined importance score, while the coloured segments represent the contributions from each method.

3.2. Prediction model based on machine learning

To address potential collinearity among the 15 candidate input variables, Spearman correlation analysis was first conducted. Variable pairs with coefficients greater than 0.70 were identified as strongly correlated. To mitigate redundancy, multi-method feature-importance scores (Random Forest, XGBoost, and

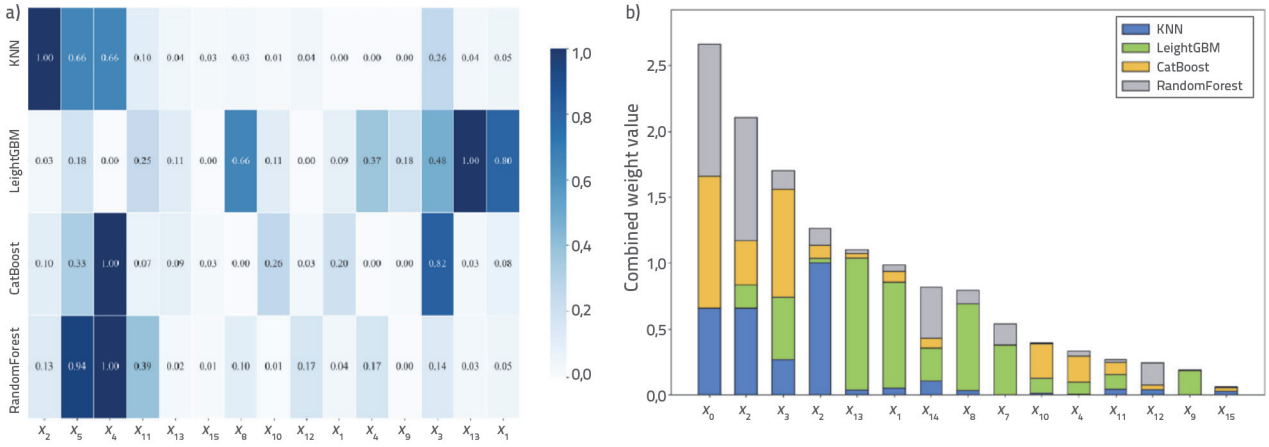

Figure 4. Importance measures of variables: a) Feature score matrix; b) Combined Importance Ranking

mutual information) were aggregated, and only the highest-ranked features were retained for subsequent modelling. In this way, the risk of multicollinearity affecting the models was minimised. Overfitting was controlled through several safeguards. Data were cleaned using Z-score analysis and Isolation Forest to remove noise and outliers. Dynamic feature selection was applied to limit the number of input variables and reduce model complexity. Model performance was validated using 5-fold cross-validation, while Bayesian optimisation was used to tune hyperparameters and enhance generalisation.

Each model was independently trained and evaluated using four standard performance metrics: R^2 (coefficient of determination), MAE (mean absolute error), RMSE (root mean square error), and MAPE (mean absolute percentage error). The corresponding expressions are provided as follows:

$$R^2 = 1 - \frac{\sum_{i=1}^{n}(y_i - \hat{y}_i)^2}{\sum_{i=1}^{n}(y_i - \bar{y})^2} \quad (1)$$

$$\text{MAE} = \frac{1}{n}\sum_{i=1}^{n}|y_i - \hat{y}_i| \quad (2)$$

$$\text{RMSE} = \sqrt{\frac{1}{n}\sum_{i=1}^{n}(y_i - \hat{y}_i)^2} \quad (3)$$

$$\text{MAPE} = \frac{1}{n}\sum_{i=1}^{n}|(y_i - \hat{y}_i)/y_i| \cdot 100\ \% \quad (4)$$

In the performance formulas, y_i represents the actual value, $\hat{y}_i$ the predicted value, $\bar{y}$ the mean value, and n the number of samples. Higher R^2 values and lower RMSE, MAE, and MAPE indicate better model performance and smaller discrepancies between the predicted and actual values.

The dataset of 152 specimens was randomly divided into training (80 %) and testing (20 %) subsets with random_state = 42 to ensure reproducibility. Summary statistics (min, max, mean, and standard deviation) for both subsets are provided in Appendix B (Supplementary Material), confirming that their distributions were consistent and statistically comparable. Table 2 summarises the model performance metrics and Figure 4 compares the predicted and actual values. Table 2 provides the R^2, MAE, RMSE, and MAPE scores for all four algorithms on both subsets, allowing a clear assessment of the model fit and generalisation ability. In the training set, KNN and CatBoost achieved near-perfect performance, with R^2 values of 0.9999 and MAE and RMSE values in the ranges of 3-8. In contrast, the RF and LightGBM yielded lower R^2 scores (0.9853 and 0.9413, respectively) and higher errors. When tested on unseen data, RF retained the highest R^2 (0.981) and controlled the MAE and RMSE to within 58.2 and 98.4%, respectively, indicating strong generalisation. CatBoost achieved a comparable R^2 of 0.9798 with a slightly higher RMSE (101.3), yet acceptable MAE and MAPE, suggesting stable predictive performance. Conversely, KNN's R^2 of KNN dropped sharply to 0.9583, with an increase in MAE and RMSE (>80 and 145, respectively), demonstrating significant overfitting. LightGBM performed the worst in this regard, with an R^2 of only 0.8357, an RMSE approaching 289, and an MAPE exceeding 30 %, failing to meet the precision requirements. Overall, Random Forest effectively balanced fit and generalisation, making it the preferred model. CatBoost is also a strong candidate with a slightly lower test accuracy. However, KNN and LightGBM exhibit significant overfitting and require parameter tuning or feature engineering before they are viable for deployment.

These results are consistent with recent ML applications in structural engineering. Taffese and Zhu [54] achieved $R^2 \approx 0.94$ and MAE ≈ 11.5 kN·m for UHPC beams, Agarwal et al. [55] reported ~18 % error in RC beam crack prediction using XGBoost, and Liu et al. [56] demonstrated that XGBoost provided the best performance ($R^2 \approx 0.99$, MAE ≈ 5.4 kN) for shear strength prediction of 174 FRCM-strengthened RC beams. Compared with these benchmarks, our RF model delivered superior accuracy (MAE ~2.6 %, $R^2 \approx 0.98$), confirming robustness and novelty for PEC beams.

Table 2. Performance of each model

Model		R^2	MAE	RMSE	MAPE	Best hyperparameters
Train	KNN	0.9999	3.1082	8.3942	1.0564	n_neighbors = 5, weights = distance
	LightGBM	0.9413	122.3384	192.5837	18.1147	num_leaves = 95, learning_rate = 0.12, n_estimators = 450
	CatBoost	0.9999	3.1497	8.3944	1.0659	iterations = 600, depth = 6, learning_rate = 0.12
	RF	0.9853	50.8568	96.3420	5.8881	n_estimators = 500, max_depth = 12, min_samples_leaf = 2
Test	KNN	0.9583	80.3360	145.6488	12.1285	n_neighbors = 5, weights = distance
	LightGBM	0.8357	166.9297	288.9514	30.4131	num_leaves = 95, learning_rate = 0.12, n_estimators = 450
	CatBoost	0.9798	58.7677	101.3208	10.3942	iterations = 600, depth = 6, learning_rate = 0.12
	RF	0.9809	58.2261	98.4188	11.4303	n_estimators = 500, max_depth = 12, min_samples_leaf = 2

Note: All models were tuned rather than relying on default settings. Hyperparameter optimisation was conducted using 5-fold cross-validation with R^2 as the scoring metric. KNN parameters were selected through a manual grid search (n_neighbors, weights), while the parameters of LightGBM, CatBoost, and Random Forest were optimised using Bayesian search within predefined ranges. The reported results correspond to the best hyperparameters identified for each model.

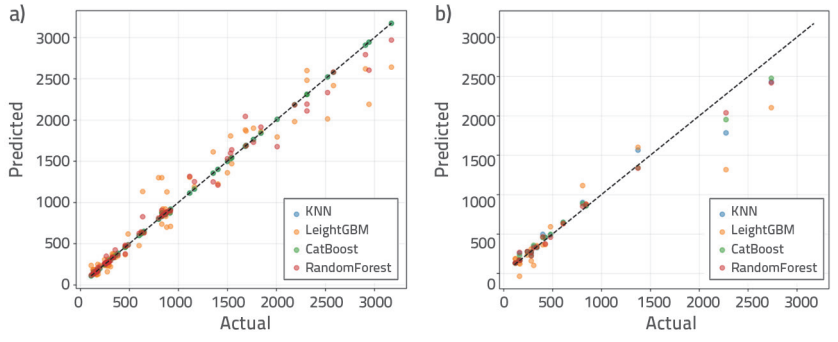

Figure 5. Comparison of true and predicted values: a) Train set; b) Test set

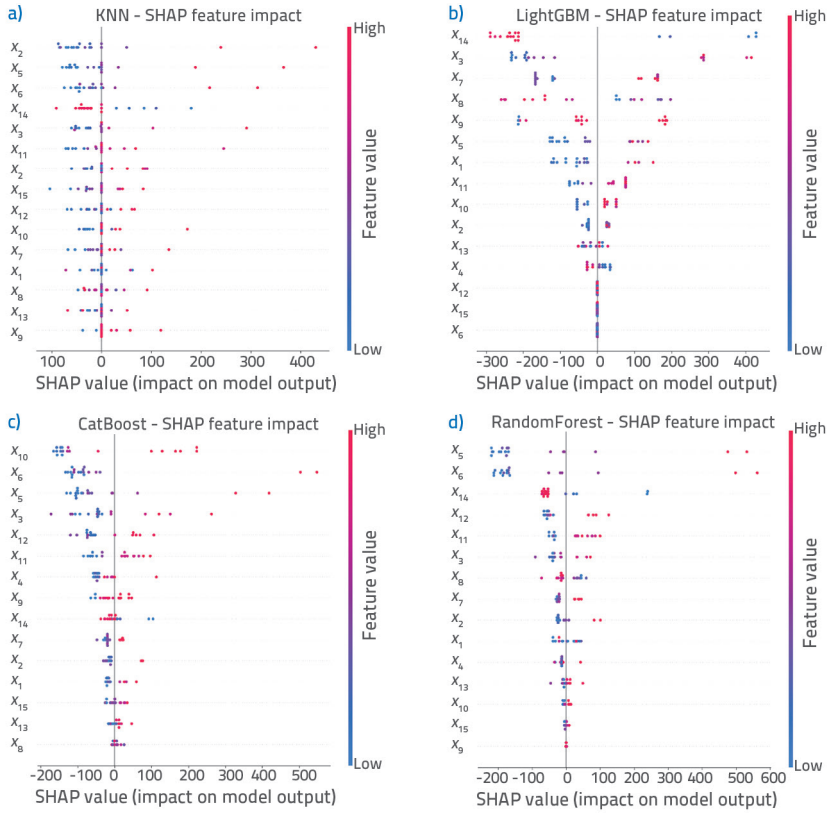

Figure 6. SHAP summary: a) KNN; b) LightGBM; c) CatBoost; d) RandomForest

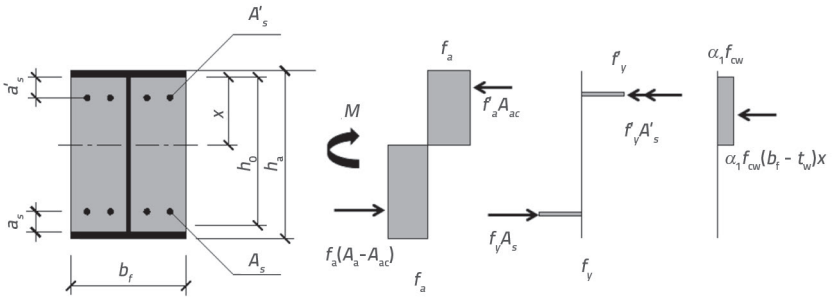

Figure 7. Section diagram and equivalent rectangular stress diagram of PEC beams

Although machine learning models offer strong predictive capability, their inherent "black-box" nature often limits interpretability and obscures the underlying decision-making process. To address this limitation, the SHAP method was applied to interpret the prediction outputs of the various models, as shown in Figure 6. In the KNN model, feature x_2 exhibited the widest range of SHAP values, predominantly positive, indicating a strong and consistent positive contribution to the predicted output, thus making it the most critical factor. Features x_5 and x_6 also had considerable influence, although their SHAP values were more symmetrically distributed, suggesting a nuanced and bidirectional effect. In the LightGBM model, feature x_{14} emerged as the dominant contributor, while x_3, x_7, x_8, and x_9 showed moderate and direction-dependent effects, indicating that their influence varied with the input values. In the CatBoost model, feature x_{10} exhibited SHAP values ranging from –200 to +550, with a strong skew towards positive contributions, indicating that higher values of x_{10} markedly increased the predicted flexural capacity. Features x_5 and x_6 followed, with more balanced SHAP distributions. For the Random Forest model, feature x_5 was the most influential, with SHAP values between –250 and +600 and a distinctly strong positive contribution. Overall, feature x_{14} was identified as the most critical predictor of flexural capacity and should receive focused attention in modelling efforts. Features x_5 and x6 showed complex and bidirectional influence and therefore warrant close monitoring. In contrast, features such as x_3, x_{11}, and x_{12} exhibited mild suppressive effects, while the remaining variables contributed only marginally to the predictive outcomes.

4. Traditional calculation method of flexural bearing capacity of PEC beams

The stress distribution and relevant parameters of the PEC beam cross-section are shown in Figure 7. As the specimen approaches its ultimate load capacity, the neutral axis progressively shifts upward and the height of the compression zone decreases. The region above the neutral axis is in compression, while the region below it is in tension, with both the flanges

and the tensile reinforcement reaching their yield strength. The formulas for calculating the flexural capacity of the PEC beams are provided in Equations (5) to (9), and the calculated results are listed in Table 6.

$$M_u = \alpha_1 f_{cw}(b_f - t_w)\frac{x^2}{2} + f_y A_s(h_a - x - 2t_f - a_s) + f_y' A_s'(x - a_s') + f_a S_{at} + f_a' S_{ac} \quad (5)$$

$$\alpha_1 f_{cw}(b_f - t_w)x + f_y' A_s' + f_a' A_{ac} - f_y A_s - f_a(A_a - A_{ac}) = 0 \quad (6)$$

$$2a_s' \le x \le \xi_b h_0 \quad (7)$$

$$\xi_b = \frac{1}{1 + \frac{f_y + f_a}{2 \times 0.003 E_s}} \quad (8)$$

$$A_{ac} = t_w x + b_f t_f \quad (9)$$

where:

M_u - the design value of the flexural capacity of the cross-section (N·mm)

f_{cw} - the axial compressive strength design value of the concrete in the web of the main steel member (N/mm²)

x - the distance from the neutral axis of the composite section to the compression edge of the concrete (mm)

α_1 - the influence coefficient of compressive stress in the compression zone

f_y, f_y' - the design values of tensile and compressive strengths of the reinforcement (N/mm²)

f_a, f_a' - the design values of tensile and compressive strengths of the main steel section of the beam (N/mm²)

A_s, A_s' - the cross-sectional areas of the tensile and compressive reinforcement (mm²)

A_a, A_{ac} - the total cross-sectional area of the main steel section and the cross-sectional area of the compression zone of the main steel section (mm²)

a_s, a_s' - the distances from the resultant force point of the tensile reinforcement to the tensile edge of the concrete and from the resultant force point of the compressive reinforcement to the compressive edge of the concrete (mm)

S_{at}, S_{ac} - the section plastic moments of the tensile and compressive areas of the main steel section relative to the plastic neutral axis of the composite section (mm³)

h_0 - the effective height of the concrete section(mm)

E_a, E_s - the elastic moduli of the main steel section and reinforcement (N/mm²)

h_a, b_f, t_w, t_f - the height, flange width, web thickness, and flange thickness of the main steel section of the beam (mm).

5. Experimental program and results analysis

5.1. Specimen design

To validate the proposed flexural capacity prediction model for PEC beams, five groups of specimens (PECB1-PECB5) were designed, fabricated, and subjected to loading tests. The specimens were designed in accordance with the T/CECS 719-2020 [57], specification. Specimen PECB1 was a primary beam, PECB2 was a secondary beam, PECB3 and PECB5 were primary beams with web openings (types 1 and 2, respectively), and PECB4 was a secondary beam with web openings. All specimens had cross-sectional heights greater than 600 mm. Structural steel was Q355-B, tie rods and anti-crack reinforcement used HRB400 steel, and the concrete strength grade was C30. The design length was 10,800 mm for specimens PECB1, PECB3, and PECB5, and 7,200 mm for specimens PECB2 and PECB4. Regarding the web openings: for specimen PECB3, the midspan openings had diameters of 400 mm, the quarter-span loading-point openings 350 mm, and the remaining openings 175 mm, with five midspan openings left unfilled; for specimen PECB4, the midspan openings had diameters of 300 mm, the quarter-span openings 200 mm, and the remaining openings 140 mm, with two midspan openings unfilled; for specimen PECB5, the midspan opening was 350 mm and the remaining openings were 175 mm, with all openings filled with concrete to facilitate casting. Additionally, the tie rod spacing was 200 mm in the pure bending zone and 150 mm in the bending-shear zone. The sectional steel ratio was calculated using only the structural steel cross-sectional area. The detailed configurations of the specimens are shown in Figure 8.

Table 3. Basic parameters of the specimen design

Specimen number	Length l_0 [mm]	Height h_a [mm]	Width b_f [mm]	Flange thickness t_f [mm]	Web thickness t_w [mm]	Steel ratio [%]
PECB1	10800	900	400	22	18	8,63
PECB2	7200	600	300	18	12	9,04
PECB3	10800	900	400	22	18	8,63
PECB4	7200	600	300	18	12	9,04
PECB5	10800	900	400	22	18	8,63

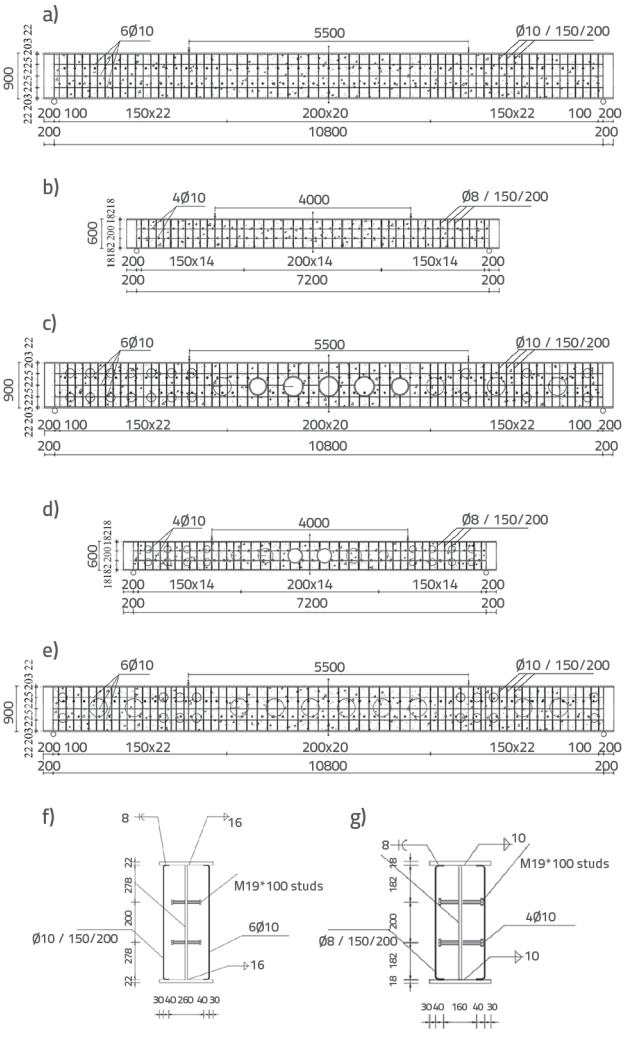

Figure 8. Schematic diagram of PEC beams: a) Specimen PECB1 elevation; b) Specimen PECB2 elevation; c) Specimen PECB3 elevation; d) Specimen PECB4 elevation; e) Specimen PECB5 elevation; f) Middle section of main beam span; g) Mid-span section of secondary beam

The material property tests for the concrete were conducted in the Building Materials Laboratory at Tongji University in accordance with the national standard *Standard for Test Methods of Physical and Mechanical Properties of Concrete* (GB/T 50081-2019) [58]. Under identical curing conditions, the concrete cube compressive strength was 31.1 MPa. The material properties of the steel were determined according to *Metallic Materials - Tensile Testing* (GB/T 228.1-2010) [59]. Standard tensile tests were performed using a universal testing machine in the Structural Engineering Laboratory at Tongji University, with the loading apparatus shown in Figure 3. All steel plates used for the specimens were taken from the same batch and were cut into proportional samples for testing. The yield strength f_y, ultimate strength f_u, and elastic modulus E of the steel materials with different thicknesses are listed in Table 4.

5.2. Loading protocol and measurement

Specimens PECB1, PECB3, and PECB5, which had larger spans and greater load-bearing capacities, were loaded monotonically using two 350-ton actuators positioned at the one-third points of the span. Specimens PECB2 and PECB4, which had smaller spans and lower capacities, were tested using a single actuator that distributed loads through a rigid beam at corresponding positions. The boundary conditions were simply supported, with sliding and fixed hinge supports at opposite ends. Loading initially followed a force-controlled regime, applied incrementally (60 kN per step for the larger specimens at 20 kN/min, and 30 kN per step for the smaller specimens at 10 kN/min) up to half of the estimated yield load. Thereafter, loading was switched to displacement control, increasing at 5 mm per step at a rate of 5 mm/min until failure, during which deflections exceeded 300 mm.

Figure 9. Specimen loading diagram: a) Loading device of PECB1, PECB3 and PECB5; b) Loading device of PECB2 and PECB4

5.3. Failure pattern of specimen

The final failure modes of specimens PECB1 to PECB5 are shown in Figs. 10 to 14. All five specimens initially developed concrete cracking, followed by yielding of both the upper and lower steel flanges, and ultimately experienced concrete spalling at the midspan top surface, with midspan deflection exceeding the

Table 4. Material properties of the steel

Number	T [mm]	f_y [MPa]	f_u [MPa]	E [MPa]
1.	12	408.13	524.31	231378
2.	18	390.81	488.79	223478
3.	22	408.49	499.13	215244

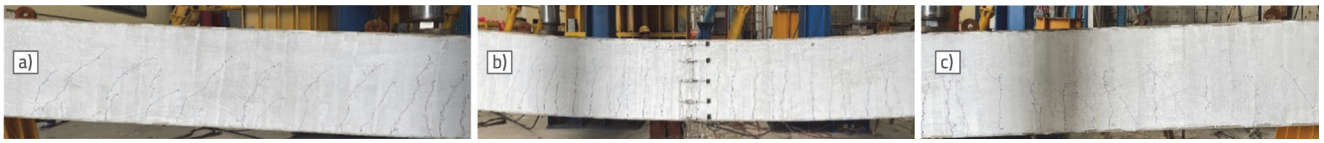

Figure 10. Final failure state of specimen PECB1: a) North side area; b) Mid-span region; c) South side area

Figure 11. Final failure state of specimen PECB2: a) North side area; b) Mid-span region; c) South side area

Figure 12. Final failure state of specimen PECB3: a) North side area; b) Mid-span region; c) South side area

Figure 13. Final failure state of specimen PECB4: a) North side area; b) Mid-span region; c) South side area

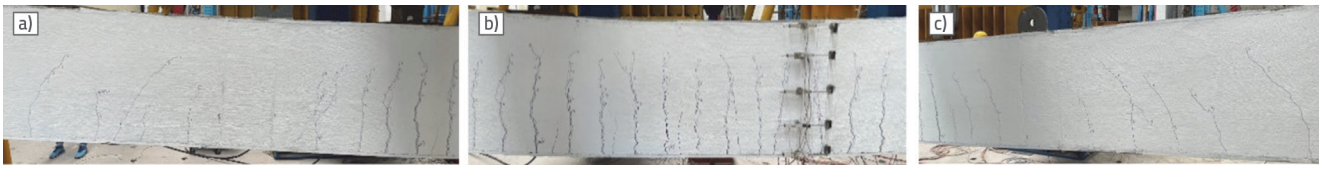

Figure 14. Final failure state of specimen PECB5: a) North side area; b) Mid-span region; c) South side area

failure criterion (1/50 of the span). Cracking typically initiated at approximately 0.11 to 0.23 Pu, with deflection and crack width increasing progressively until serviceability limits were exceeded at around 0.69 to 0.85 P_u. For specimens PECB3 and PECB4, the presence of web openings significantly influenced the load-transfer mechanism, producing distinctive radiating cracks extending downward from the openings, wider crack formation, and more severe concrete spalling and bulging above the openings.

5.4. Load-midspan deflection curve

The load-midspan deflection curves for the specimens are shown in Figure 15 and exhibit two distinct phases.

- **Elastic stage:** Before yielding of the tensile flange, the primary steel section and reinforcement restrain the concrete, resulting in slow crack propagation and negligible change in sectional stiffness. The load-midspan deflection response is predominantly linear.
- **Elasto-plastic stage:** Once the tensile flange yields, the specimen enters the elasto-plastic phase. Cracks in the abdominal concrete propagate rapidly, and its contribution to structural integrity diminishes, reducing sectional stiffness. The load-midspan deflection curve develops inflection points and transitions to nonlinear behaviour, with increased midspan deflection and more pronounced bending. As the load continues to increase, the lower flange of the primary steel section enters strain hardening, preventing a reduction in flexural capacity. When the upper flange yields, partial spalling of the top concrete at midspan occurs, and deflection reaches the allowable limit, leading to test termination.

Comparison of the load-midspan deflection curves for specimens with and without web openings shows minimal differences in initial stiffness. Although the openings reduce the stiffness of the primary steel section, this effect is offset by concrete infill and reinforcement. After yielding, the load-bearing capacity of PECB1 was slightly higher than that of PECB3 and PECB5; however, their ultimate capacities were essentially similar. The curves of PECB2 and PECB4 also displayed no significant differences in trend. These observations indicate that web openings slightly reduce load-bearing capacity but have limited overall influence. This is because the flexural capacity of PEC

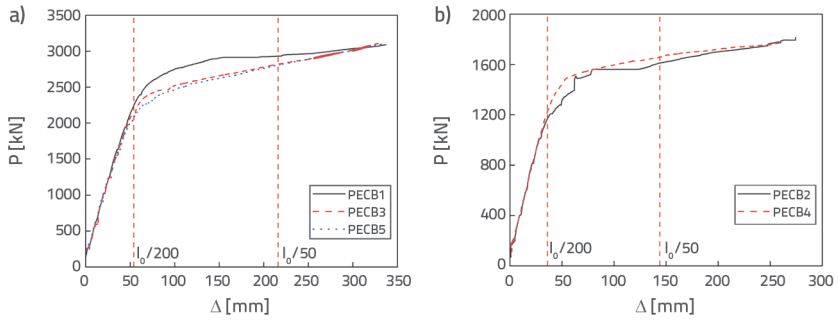

Figure 15. Load-midspan deflection curve: a) PECB1, PECB3 and PECB5; b) PECB2 and PECB4

beams is governed primarily by the steel flanges, web, and concrete, with the web itself playing a relatively minor role.

5.5. Bearing capacity analysis

Based on the load-midspan deflection curves of the specimens, the load-bearing capacities and displacements at characteristic points are summarised in Table 5. The theoretical cracking load P'_{cr} was calculated using the *Technical Specification for Partially Encased Composite Steel-Concrete Structures* (T/CECS 719-2020) [37], while the actual cracking load P_{cr} was obtained experimentally. The theoretical yield load P'_{y} was calculated using the yield stress from material tests according to the edge-yield criterion, and the actual yield load P_{y} was determined experimentally using the Park method. The theoretical ultimate load P'_{u} was derived using the full-section plasticity criterion, whereas the actual ultimate load P_{u} was measured experimentally. The ductility coefficient μ was used to evaluate the ductility performance of the specimens and is defined as $\mu = \Delta_u/\Delta_y$, where Δ_u is the ultimate displacement, and Δ_y is the yield displacement.

As shown in Table 3, the experimental load values at the characteristic points of the specimens were higher than the calculated values, indicating that the load-bearing capacity can be determined using the edge yield criterion and the full-section plasticity criterion. The cracking load of the specimens ranged from 0.1 P_u to 0.2 P_u, indicating early cracking. This was likely due to the presence of initial cracks in the concrete. However, the crack development satisfied the specification requirements, and the load-bearing capacity exceeded 0.7 P_u at the normal serviceability limit state. The overstrength ratio of the specimens ranged from 1.18 to 1.30, indicating that the specimens retained a certain strength reserve after reaching the yield load. At the end of the tests, the load-bearing capacity of all specimens did not decrease; however, the stiffness degradation was significant, and the deflection reached $l_0/50$. All specimens exhibited excellent ductility, with ductility coefficients exceeding 4.0. Compared with specimen PECB1, the yield strength of specimens PECB3 and PECB5 decreased by 6.0 % and 8.4 %, respectively, while their yield displacements increased by 5.2 % and 6.0 %, respectively. The yield strength and yield displacement of specimens PECB2 and PECB4 showed minimal differences, indicating that PEC beams are more significantly affected by web openings in the steel section.

5.6. Verification of calculation methods

Based on the machine learning models trained in Chapter 2, a predictive analysis was conducted to estimate the flexural capacity of PEC beams used in the experimental tests. These predictions were compared with the theoretical values calculated using the full-section plastic theory (Equation 5), with results summarised in Table 6.

For specimens PECB1-PECB5, the traditional formula exhibited significant conservativeness, overestimating the ultimate moment by up to 23 %. Among the machine learning models:

- KNN showed both over- and underestimations (–23 % to +6 %), indicating instability,
- LightGBM consistently overestimated the results (errors of 8-13 %), reflecting bias.
- CatBoost demonstrated higher accuracy, maintaining prediction errors below 5 % for most specimens.

Table 5. Bearing capacity and displacement at characteristic points

Specimen number	Cracking load [kN]		Yielding load [kN]		Δ_y [mm]	P_y / P'_y	Ultimate load [kN]		Δ_u [mm]	P_u / P'_u	P_u / P_y	μ
	P'_{cr}	P_{cr}	P'_y	P_y			P'_u	P_u				
PECB1	155.4	348.2	2185.4	2605.9	77.75	1.19	2734.5	3090.2	336.88	1.07	1.19	4.33
PECB2	88.7	193.5	1241.6	1504.2	63.19	1.21	1474.4	1813.6	274.38	1.32	1.21	4.34
PECB3	155.4	339.9	2185.4	2450.3	81.82	1.12	2734.5	3107.9	328.44	1.31	1.27	4.01
PECB4	88.7	201.5	1241.6	1511.1	60.45	1.22	1474.4	1776.7	261.27	1.14	1.18	4.32
PECB5	155.4	323.4	2185.4	2386.6	82.43	1.09	2734.5	3100.1	334.16	1.13	1.30	4.05

Table 6. Comparison of calculated and experimental flexural capacities

Specimen number	KNN		LightGBM		CatBoost		RF		Calculated value		Testing values [MPa]
	Values [MPa]	Error [%]	Values [MPa]	Error [%]	Values [MPa]	Error [%]	Values [MPa]	Error [%]	Values [MPa]	Error [%]	
PECB1	6658.6	-19.7	4828.8	13.2	4510.0	18.9	5587.8	-0.5	4922.1	11.5	5561.28
PECB2	2621.7	-14.2	2107.1	8.2	2250.6	2.0	2348.9	-2.3	1769.3	23.0	2296.32
PECB3	5244.2	6.3	4935.3	11.8	5446.0	2.6	5747.4	-2.7	4922.1	12.0	5594.22
PECB4	2622.9	-23.0	2414.4	-13.2	2028.5	4.9	2034.5	4.6	1769.3	17.0	2132.04
PECB5	5244.2	6.0	4935.3	11.6	5446.0	2.4	5747.4	-3.0	4922.1	11.8	5580.18

- Random Forest (RF) yielded the most accurate and stable results, with absolute errors below 5 % for all specimens.

When evaluated using the mean absolute percentage error (MAPE) across all samples, RF achieved the best performance (~2.6 %), followed by CatBoost (~6 %), while LightGBM (~11.6 %) and KNN (~13.8 %) exhibited larger errors. The conventional formula performed worst, with an average error of approximately 15 %. Consequently, RF is recommended as the primary predictive model, with CatBoost as a secondary option, whereas KNN and LightGBM require further optimisation to improve predictive stability.

6. Conclusions

This study conducted four-point bending tests on PEC beams to investigate the effects of parameters such as section dimensions, web openings, and opening configurations on failure characteristics, deflection behaviour, flexural capacity, ductility, and sectional strain distribution. The main conclusions are as follows:

1. Fifteen critical variables influencing the flexural capacity of PEC beams were identified, and four machine learning models were evaluated using a curated database. Among these models, the RF algorithm demonstrated the highest testing accuracy while effectively mitigating overfitting. It outperformed CatBoost, KNN, and LightGBM, indicating that RF is the most suitable model for predicting the flexural behaviour of PEC beams.
2. The interpretability of the RF model was further enhanced by SHAP analysis. The results revealed that reinforcement ratio (x 14), flange thickness (x 5), and web thickness (x 6) were the most influential variables. A higher reinforcement ratio consistently produced strong positive SHAP values, indicating its direct contribution to increased flexural capacity. Flange and web thickness exhibited substantial but bidirectional effects, reflecting the interaction between stiffness enhancement and sectional balance. Other parameters, such as web opening size (x 3) and concrete strength (x 11), displayed smaller SHAP magnitudes, indicating secondary influence.
3. Experimental tests confirmed that web openings in PEC beams have a weakening effect on the load-bearing capacity of the specimens, although the overall impact is limited. Compared with specimen PECB1, the yield strength of specimens PECB3 and PECB5 decreased by 6.0 % and 8.4 %, respectively, while the yield strength of specimens PECB2 and PECB4 showed no significant difference. All specimens exhibited ductility coefficients above 4.0, demonstrating excellent ductility in PEC beams.
4. A comparative analysis of prediction errors across the five groups of specimens showed that the RF model delivered the highest accuracy, with a mean absolute error of approximately 2.6 %. This performance was significantly better than that of CatBoost (~6 %), LightGBM (~11.6 %), KNN (~13.8 %), and the conventional design formula (~15 %). Accordingly, RF is identified as the most reliable model for predicting the flexural capacity of PEC beams.

Acknowledgements

The authors thank Hongxin Liu, Ping Yang, and Yaming Li for their contributions to the conceptualisation, methodology, and funding acquisition for the research. Shuizhong Jia is acknowledged for preparing the original draft, and Xiaomeng Xie is recognised for their contributions to writing, review, and editing. The authors also thank Yukun Yang from Shanghai Jieyi Construction Technology Co., Ltd. and Jie Li from Sanda University and Tongji University for their valuable contributions to this research, despite not being listed as authors. Their efforts in methodology and software development were instrumental to the completion of this study. This study was supported by the Scientific Research Project of the Shanghai Science and Technology Commission (21DZ1203002) and the Project of East China Construction Group Co., Ltd. (Class 20-1-0073-Junction).

REFERENCES

[1] Huang, H., Xue, C., Zhang, W., et al.: Torsion design of CFRP-CFST columns using a data-driven optimization approach, Engineering Structures, 251 (2022), Paper 113479, https://doi.org/10.1016/j.engstruct.2021.113479

[2] Correia, A.J.P.M., Rodrigues, J.P.C.: Fire resistance of partially encased steel columns with restrained thermal elongation, Journal of Constructional Steel Research, 67 (2011) 4, pp. 593-601, https://doi.org/10.1016/j.jcsr.2010.12.002

[3] Chen, Q., Hou, Z., Hao, T., et al.: Web buckling analysis of steel-concrete composite beams considering flange restraints, Građevinar, 77 (2025) 2, pp. 113-123, https://doi.org/10.14256/JCE.3693.2023

[4] Tian, Y., Liu, D., Chen, X., et al.: Damage evolution of steel-UHPC composite beams using AE and DIC techniques, Journal of Constructional Steel Research, 224 (2025), Paper 109163, https://doi.org/10.1016/j.jcsr.2024.109163

[5] Jakovljević, I., Spremić, M., Marković, Z.: Demountable composite steel-concrete floors: A state-of-the-art review, Građevinar, 73 (2021) 3, pp. 249-236, https://doi.org/10.14256/JCE.2932.2020

[6] Zhang, A.L., Li, S.H., Jiang, Z.Q., et al.: Design theory of earthquake-resilient prefabricated sinusoidal corrugated web beam-column joint, Engineering Structures, 150 (2017), pp. 665-673, https://doi.org/10.1016/j.engstruct.2017.07.088

[7] Chen, Z., Niu, X., Liu, J., et al.: Seismic study on an innovative fully-bolted beam-column joint in prefabricated modular steel buildings, Engineering Structures, 234 (2021), Paper 111875, https://doi.org/10.1016/j.engstruct.2021.111875

[8] De Angelis, A., Pecce, M.R., Logorano, G.: Evaluation of the plastic hinge length of steel-concrete composite beams under hogging moment, Engineering Structures, 191 (2019), pp. 674-685, https://doi.org/10.1016/j.engstruct.2019.04.077

[9] Yao, Y., Huang, H., Zhang, W., et al.: Seismic performance of steel-PEC spliced frame beam, Journal of Constructional Steel Research, 197 (2022), Paper 107456, https://doi.org/10.1016/j.jcsr.2022.107456

[10] Chen, Y., Li, W., Fang, C.: Performance of partially encased composite beams under static and cyclic bending, Structures, 9 (2017) 2, pp. 29-40, https://doi.org/10.1016/j.istruc.2016.09.004

[11] Jiang, Y., Hu, X., Hong, W., et al.: Experimental study and theoretical analysis of partially encased continuous composite beams, Journal of Constructional Steel Research, 117 (2016), pp. 152-160, https://doi.org/10.1016/j.jcsr.2015.10.009

[12] Wang, Z., Ye, Y., Ma, Y., et al.: Experimental and finite element flexural performance study of HPEC beam, Journal of Constructional Steel Research, 211 (2023), Paper 108189, https://doi.org/10.1016/j.jcsr.2023.108189

[13] Ahn, J.K., Lee, C.H.: Fire behavior and resistance of partially encased and slim-floor composite beams, Journal of Constructional Steel Research, 129 (2017), pp. 276-285, https://doi.org/10.1016/j.jcsr.2016.11.018

[14] He, J., Wang, S., Liu, Y., et al.: Mechanical behavior of a partially encased composite girder with corrugated steel web: Interaction of shear and bending, Engineering, 3 (2017) 6, pp. 806-816, https://doi.org/10.1016/j.eng.2017.11.005

[15] Piloto, P.A.G., Ramos-Gavilán, A.B., Gonçalves, C., et al.: Experimental bending tests of partially encased beams at elevated temperatures, Fire Safety Journal, 92 (2017), pp. 23-41, https://doi.org/10.1016/j.firesaf.2017.05.014

[16] Nakamura, S., Momiyama, Y., Hosaka, T., et al.: New technologies of steel/concrete composite bridges, Journal of Constructional Steel Research, 58 (2002) 1, pp. 99-130, https://doi.org/10.1016/s0143-974x(01)00030-x

[17] He, J., Liu, Y., Lin, Z., et al.: Shear behavior of partially encased composite I-girder with corrugated steel web: Numerical study, Journal of Constructional Steel Research, 79 (2012), pp. 166-182, https://doi.org/10.1016/j.jcsr.2012.07.018

[18] He, J., Liu, Y., Chen, A., et al.: Bending behavior of concrete-encased composite I-girder with corrugated steel web, Thin-walled structures, 74 (2014), pp. 70-84, https://doi.org/10.1016/j.tws.2013.08.003

[19] De Nardin, S., El Debs, A.L.H.C.: Study of partially encased composite beams with innovative position of stud bolts, Journal of Constructional Steel Research, 65 (2009) 2, pp. 342-350, https://doi.org/10.1016/j.jcsr.2008.03.021

[20] Kindmann, R., Bergmann, R., Cajot, L.G., et al.: Effect of reinforced concrete between the flanges of the steel profile of partially encased composite beams, Journal of Constructional Steel Research, 27 (1993) 1-3, pp. 107-122, https://doi.org/10.1016/0143-974x(93)90009-h

[21] Barros, J.A.O., Figueiras, J.A.: Flexural behavior of SFRC: testing and modeling, Journal of materials in civil engineering, 11 (1999) 4, pp. 331-339, https://doi.org/10.1061/(ASCE)0899-1561(1999)11:4(331)

[22] Li, V.C.: Engineered cementitious composites (ECC) material, structural, and durability performance, 2008.

[23] Yoo, D.Y, Yoon, .S.: Structural performance of ultra-high-performance concrete beams with different steel fibers, Engineering Structures, 102 (2015), pp. 409-423, https://doi.org/10.1016/j.engstruct.2015.08.029

[24] Hao, N., Yang, Y., Xue, Y., et al:. Shear performance of partially encased composite beams with high-strength steel and UHPC, Journal of Constructional Steel Research, 211 (2023), Paper 108217, https://doi.org/10.1016/j.jcsr.2023.108217

[25] Zhao, B., Huo, H., Ran, C., et al.: Flexural behavior of castellated partially encased composite (PEC) beams, Journal of Constructional Steel Research, 214 (2024), Paper 108509, https://doi.org/10.1016/j.jcsr.2024.108509

[26] Guvel, S.T., Budak, A., Karatas, I.: Novel meta-ensemble modelling approach and comparison of machine-learning models for rebar price estimation, GRAĐEVINAR, 77 (2025) 1, pp. 27-41, https://doi.org/10.14256/JCE.4029.2024

[27] Kovačević, M., Ivanišević, N., Petronijević, P., Despotović, V.: Construction cost estimation of reinforced and prestressed concrete bridges using machine learning, GRAĐEVINAR, 73 (2021) 1, pp. 1-13, https://doi.org/10.14256/JCE.2738.2019

[28] Fang, X., Wang, C., Li, H., et al.: Influence of mesoscopic pore characteristics on the splitting-tensile strength of cellular concrete through deep-learning based image segmentation, Construction and Building Materials, 315 (2022), Paper 125335, https://doi.org/10.1016/j.conbuildmat.2021.125335

[29] Rabi, M., Jweihan, Y.S., Abarkan, I., et al.: Machine learning-driven web-post buckling resistance prediction for high-strength steel beams with elliptically-based web openings, Results in Engineering, 21 (2024), Paper 101749, https://doi.org/10.1016/j.rineng.2024.101749

[30] Ma, C., Chi, J., Kong, F., et al.: Prediction on the seismic performance limits of reinforced concrete columns based on machine learning method, Soil Dynamics and Earthquake Engineering, 177 (2024), Paper 108423, https://doi.org/10.1016/j.soildyn.2023.108423

[31] Liu, T., Wang, Z., Zeng, J., et al.: Machine-learning-based models to predict shear transfer strength of concrete joints, Engineering Structures, 249 (2021), Paper 113253, https://doi.org/10.1016/j.engstruct.2021.113253

[32] Zhang, T., Xu, W., Wang, S., et al.: Seismic response prediction of a damped structure based on data-driven machine learning methods, Engineering Structures, 301 (2024), Paper 117264, https://doi.org/10.1016/j.engstruct.2023.117264

[33] Gatheeshgar, P., Ranasinghe, R.S.S., Simwanda, L., et al.: Machine learning prediction of web-crippling strength in cold-formed steel beams with staggered slotted perforations, Structures, 71 (2025), Paper 108079, https://doi.org/10.1016/j.istruc.2024.108079

[34] Alshboul, O., Almasabha, G., Shehadeh, A., et al.: A comparative study of LightGBM, XGBoost, and GEP models in shear strength management of SFRC-SBWS, Structures, 61 (2024), Paper 106009, https://doi.org/10.1016/j.istruc.2024.106009

[35] Taffese, W.Z., Zhu, Y.: Explainable machine learning for predicting flexural capacity of reinforced UHPC beams, Engineering Structures, 343 (2025), Paper 121188, https://doi.org/10.1016/j.engstruct.2025.121188

[36] Wang, C., Guo, H., Jiang, C., et al. Physics guided neural network framework for predicting shear strength of corroded reinforced concrete beams, Engineering Failure Analysis, (2025), Paper 109970, https://doi.org/10.1016/j.engfailanal.2025.109970

[37] Yan, H.: Test and Theoretical Research on Flexural Performance of PEC Honeycomb Beams with Different Structural Forms, Shandong University, 2021. (in Chinese)

[38] Li, Q.Z.: Test and Theoretical Research on the Bending Performance of Open-Web PEC Beams, Zhengzhou University, 2022. (in Chinese)

[39] Zhao, B.D., Zhang, X.F., Wang, W., et al.: Experimental Study on Flexural Performance of Partially Coated Honeycomb steel-concrete composite Beams , Journal of Building Structures, 44 (2023) 7, pp. 161-171. (in Chinese)

[40] Zou, C.R., Ke, M.Z., Zhou, H.B., et al.: The influence of web opening of main steel components on the performance of partially coated steel-concrete composite beams , Building Structures, 53 (2023) S1, pp. 1842-1847. (in Chinese)

[41] Wang, N., Hou, H., Wang, Y., et al.: Flexural behavior of partially encased cellular beams: Tests and design implications, Engineering Structures, 293 (2023), Paper 116631, https://doi.org/10.1016/j.engstruct.2023.116631

[42] Liang, J., Zou, W., Wang, C., et al.: Flexural performance of partially encased steel-concrete composite beams with web opening, Structures, 64 (2024), Paper 106666, https://doi.org/10.1016/j.istruc.2024.106666

[43] Ye, Y., Yao, Y., Liao, H., et al.: Flexural performance of hollow-core partially-encased composite beams, Journal of Building Engineering, 45 (2022), Paper 103432, https://doi.org/10.1016/j.jobe.2021.103432

[44] Bai, Y.Z., Cheng, X., An, Y., et al.: Experimental Study on Flexural Performance of Light Steel - Lightweight Aggregate Concrete PEC Beams, Engineering Mechanics, 3 (2025), pp. 1-13. (in Chinese)

[45] Zhang, J.X.: Research on the Bearing Capacity of Lightweight Aggregate Concrete PEC Beams, Taiyuan University of Technology, 2023. (in Chinese)

[46] He, Z.L.: Research on the Bending Performance of Prestressed Partially Wrapped Composite Beams, Guangxi University of Science and Technology, 2016. (in Chinese)

[47] Qi, H., Li, J., Wang, X., et al.: Experimental Study on Bending Performance of PEC Beam with Sinusoidal Waveform Web , Steel Structure, 38 (2023) 6, pp. 22-31. (in Chinese)

[48] Chu, L., Guo, X., Li, J., et al.: Experimental study on the flexural behavior of partially encased composite beams with corrugated steel webs, Advances in Structural Engineering, 27 (2024) 6, pp. 1071-1084, https://doi.org/10.1177/13694332241242974

[49] Liao, H.Y.: Research on the Mechanical Performance of Hollow Part Outsourced Concrete Composite Beams, Chang 'an University, 2023. (in Chinese)

[50] Yan, J.: Research on the Bending Performance of Normal Sections of Double-C Light Steel Partially Wrapped FSLC Composite Beams, Inner Mongolia University of Science and Technology, 2022. (in Chinese)

[51] Yao, Y.F.: Research on the Mechanical Properties and Design Methods of Concrete Composite Beams with Hollow Part Cladding, Chang 'an University, 2023. (in Chinese)

[52] Deng, J.: Research on Flexural Performance of Partially Coated Concrete Beams with Honeycomb Steel, East China University of Technology, 2024. (in Chinese)

[53] Deng, C.J.: Experimental and Theoretical Research on Bending Performance of Wave-Web PEC Beams, Zhengzhou University, 2023. (in Chinese)

[54] Taffese, W.Z., Zhu, Y.: Explainable machine learning for predicting flexural capacity of reinforced UHPC beams, Engineering Structures, 343(2025), Paper 121188, https://doi.org/10.1016/j.engstruct.2025.121188

[55] Agarwal, H., Shariff, M.N., Mangalathu, S.: Prediction of flexural crack width of reinforced concrete beams using interpretable machine learning algorithms, Construction and Building Materials, 485 (2025), Paper 141628, https://doi.org/10.1016/j.conbuildmat.2025.141628

[56] Liu, X., Figueredo, G.P., Gordon, G.S.D., et al.: Data-driven shear strength prediction of RC beams strengthened with FRCM jackets using machine learning approach, Engineering Structures, 325 (2025), Paper 119485, https://doi.org/10.1016/j.engstruct.2024.119485

[57] Technical specification for partially clad steel-concrete composite structures: T/CECS 719-2020, Beijing: China Architecture and Construction Press, 2020. (in Chinese)

[58] Test method standard for physical and mechanical properties of concrete: GB/T50081-2019, Beijing: Standards Press of China, 2019. (in Chinese)

[59] Tensile test method for metal materials at room temperature GB/T 228-2002, Beijing: Standards Press of China, 2002. (in Chinese)

Appendix A

References	Number	x_1	x_2	x_3	x_4	x_5	x_6	x_7	x_8	x_9	x_{10}	x_{11}	x_{12}	x_{13}	x_{14}	x_{15}	Y
[37]	1	150.00	300.00	5.00	3.00	95.00	95.00	226.08	0.50	464.70	296.00	318.00	28.82	0.05	0.95	850	104.50
	2	150.00	300.00	5.00	3.00	95.00	95.00	226.08	0.50	464.70	296.00	318.00	28.82	0.05	0.95	850	120.40
	3	150.00	300.00	5.00	3.00	95.00	95.00	307.72	0.68	422.20	296.00	318.00	28.82	0.05	0.95	850	106.30
	4	150.00	300.00	5.00	3.00	95.00	95.00	226.08	0.50	464.70	296.00	318.00	28.82	0.05	0.95	850	107.10
[38]	5	200.00	400.00	10.00	6.00	60.00	60.00	157.00	0.20	390.81	390.81	408.13	42.96	0.06	0.94	1600	319.04
	6	200.00	500.00	10.00	6.00	75.00	75.00	157.00	0.16	391.81	390.81	408.13	42.96	0.05	0.95	1600	412.54
	7	200.00	400.00	8.00	6.00	60.00	60.00	157.00	0.20	392.81	415.50	408.13	42.96	0.05	0.95	1600	236.42
	8	200.00	400.00	10.00	6.00	90.00	90.00	157.00	0.20	393.81	390.81	408.13	42.96	0.06	0.94	1600	324.42
	9	200.00	400.00	8.00	12.00	60.00	60.00	157.00	0.20	394.81	415.50	408.13	42.96	0.06	0.94	1600	307.52
	10	200.00	500.00	8.00	12.00	75.00	75.00	157.00	0.16	395.81	415.50	408.13	42.96	0.05	0.95	1600	398.98
	11	200.00	400.00	6.00	12.00	60.00	60.00	157.00	0.20	396.81	408.13	408.13	42.96	0.05	0.95	1600	266.56
	12	200.00	400.00	8.00	12.00	90.00	90.00	157.00	0.20	397.81	415.50	408.13	42.96	0.07	0.93	1600	303.74
	13	200.00	400.00	10.00	6.00	60.00	60.00	157.00	0.20	390.81	390.81	408.13	42.96	0.06	0.94	1600	374.16
	14	200.00	400.00	10.00	6.00	45.00	45.00	157.00	0.20	390.81	390.81	408.13	42.96	0.06	0.94	1600	388.56
	15	200.00	400.00	10.00	6.00	45.00	45.00	157.00	0.20	390.81	390.81	408.13	42.96	0.06	0.94	1600	394.16
	16	200.00	400.00	10.00	6.00	60.00	60.00	157.00	0.20	390.81	390.81	408.13	30.00	0.06	0.94	1600	380.18
	17	200.00	400.00	10.00	6.00	60.00	60.00	157.00	0.20	390.81	390.81	408.13	50.00	0.06	0.94	1600	386.82
	18	200.00	400.00	10.00	6.00	60.00	60.00	157.00	0.20	390.81	260.54	272.09	42.96	0.06	0.94	1600	222.75
	19	200.00	400.00	10.00	6.00	60.00	60.00	157.00	0.20	390.81	586.22	612.20	42.96	0.06	0.94	1600	313.06
	20	200.00	400.00	10.00	8.00	60.00	60.00	157.00	0.20	390.81	390.81	408.13	42.96	0.06	0.94	1600	403.18
[39]	21	175.00	200.00	6.00	5.00	44.00	44.00	157.00	0.45	481.50	361.50	376.20	45.61	0.07	0.93	900	107.40
	22	175.00	300.00	6.00	5.00	44.00	44.00	157.00	0.30	482.50	361.50	376.20	45.61	0.05	0.95	900	193.70
	23	175.00	300.00	6.00	5.00	44.00	44.00	157.00	0.30	483.50	361.50	376.20	45.61	0.05	0.95	900	165.00
[40]	24	175.00	350.00	6.00	5.00	44.00	44.00	157.00	0.26	484.50	361.50	376.20	45.61	0.04	0.96	900	187.10
	25	175.00	300.00	6.00	5.00	44.00	44.00	157.00	0.30	485.50	361.50	376.20	46.61	0.05	0.95	900	193.70
	26	175.00	300.00	6.00	5.00	144.00	144.00	157.00	0.30	486.50	361.50	376.20	47.61	0.07	0.93	900	165.00
[41]	27	150.00	300.00	4.50	3.20	45.50	45.50	226.08	0.50	464.70	296.00	318.00	19.30	0.04	0.96	850	109.80
	28	150.00	300.00	4.50	3.20	45.50	45.50	307.72	0.68	422.20	296.00	318.00	19.30	0.04	0.96	850	120.90
	29	150.00	300.00	4.50	3.20	45.50	45.50	226.08	0.50	464.70	296.00	318.00	19.30	0.04	0.96	850	111.40
	30	150.00	300.00	4.50	3.20	45.50	45.50	226.08	0.50	464.70	296.00	318.00	19.30	0.04	0.96	850	110.90
[25]	31	175.00	300.00	6.00	5.00	44.00	44.00	157.00	0.30	481.50	361.50	376.20	43.30	0.05	0.95	900	165.00
	32	175.00	350.00	6.00	5.00	19.00	19.00	157.00	0.26	481.50	361.50	376.20	43.30	0.04	0.96	900	187.10
	33	175.00	300.00	6.00	5.00	25.00	44.00	157.00	0.30	481.50	361.50	376.20	43.30	0.05	0.95	900	132.30
[42]	34	150.00	194.00	9.00	6.00	38.00	38.00	0.00	0.00	0.00	312.00	320.00	32.90	0.11	0.89	400	89.19
	35	150.00	194.00	9.00	6.00	38.00	38.00	0.00	0.00	0.00	312.00	320.00	46.90	0.11	0.89	400	99.74
	36	150.00	194.00	9.00	6.00	38.00	38.00	0.00	0.00	0.00	312.00	320.00	32.90	0.11	0.89	400	80.13
	37	150.00	194.00	9.00	6.00	38.00	38.00	0.00	0.00	0.00	312.00	320.00	32.90	0.11	0.89	400	85.02
	38	150.00	194.00	9.00	6.00	38.00	38.00	0.00	0.00	0.00	312.00	320.00	32.90	0.11	0.89	400	78.35
	39	150.00	191.00	9.00	6.00	38.00	38.00	0.00	0.00	0.00	312.00	320.00	32.90	0.09	0.91	400	73.53
	40	150.00	189.00	9.00	6.00	38.00	38.00	0.00	0.00	0.00	312.00	320.00	32.90	0.08	0.92	400	64.87
	41	150.00	194.00	9.00	6.00	88.00	88.00	0.00	0.00	0.00	312.00	320.00	32.90	0.13	0.87	400	98.22

Appendix A - continuation

References	Number	x_1	x_2	x_3	x_4	x_5	x_6	x_7	x_8	x_9	x_{10}	x_{11}	x_{12}	x_{13}	x_{14}	x_{15}	y
[43]	42	250.00	400.00	8.00	10.00	192.00	192.00	401.92	0.40	390.00	400.00	420.00	61.90	0.08	0.38	1250	576.88
	43	250.00	400.00	8.00	10.00	192.00	192.00	401.92	0.40	390.00	400.00	420.00	82.30	0.08	0.47	1250	553.75
	44	250.00	400.00	8.00	10.00	192.00	192.00	401.92	0.40	390.00	400.00	420.00	61.90	0.08	0.38	1250	560.63
	45	250.00	400.00	8.00	10.00	192.00	192.00	200.96	0.20	390.00	400.00	420.00	61.90	0.08	0.92	1250	612.50
[44]	46	160.00	300.00	8.00	4.00	142.00	142.00	157.00	0.33	454.62	356.80	464.24	33.10	0.08	0.92	900	305.00
	47	160.00	300.00	8.00	4.00	142.00	142.00	157.00	0.33	454.62	356.80	464.24	33.10	0.08	0.92	900	283.10
	48	200.00	300.00	6.00	4.00	144.00	144.00	157.00	0.26	454.62	325.75	464.24	33.10	0.06	0.94	900	226.30
	49	200.00	300.00	6.00	4.00	144.00	144.00	157.00	0.26	454.62	325.75	464.24	33.10	0.06	0.94	900	215.60
	50	250.00	400.00	6.00	4.00	194.00	194.00	157.00	0.16	454.62	325.75	464.24	33.10	0.05	0.95	900	432.80
[45]	51	250.00	400.00	6.00	4.00	194.00	194.00	157.00	0.16	454.62	325.75	464.24	33.10	0.05	0.95	900	405.60
	52	200.00	300.00	6.00	4.00	144.00	144.00	157.00	0.26	454.62	317.17	424.57	33.10	0.06	0.94	900	226.29
	53	200.00	300.00	6.00	4.00	144.00	144.00	157.00	0.26	454.62	317.17	424.57	33.10	0.06	0.94	900	215.64
	54	200.00	300.00	6.00	4.00	144.00	144.00	157.00	0.26	454.62	317.17	424.57	33.10	0.06	0.94	900	224.58
	55	200.00	300.00	6.00	4.00	144.00	144.00	157.00	0.26	454.62	317.17	424.57	41.45	0.06	0.94	900	255.14
	56	160.00	300.00	6.00	4.00	144.00	144.00	157.00	0.33	454.62	317.17	424.57	33.10	0.06	0.94	900	203.96
[46]	57	150.00	194.00	9.00	6.00	88.00	88.00	0.00	0.00	0.00	305.00	305.00	31.45	0.13	0.87	950	88.30
	58	150.00	194.00	9.00	6.00	88.00	88.00	0.00	0.00	0.00	305.00	305.00	31.45	0.13	0.87	950	113.57
	59	150.00	194.00	9.00	6.00	88.00	88.00	0.00	0.00	0.00	305.00	305.00	31.45	0.13	0.87	950	111.91
	60	150.00	194.00	9.00	6.00	88.00	88.00	0.00	0.00	0.00	305.00	305.00	31.45	0.13	0.87	950	107.46
	61	200.00	200.00	12.00	8.00	88.00	88.00	0.00	0.00	0.00	305.00	305.00	31.45	0.16	0.84	950	160.17
	62	200.00	200.00	12.00	8.00	88.00	88.00	0.00	0.00	0.00	305.00	305.00	31.45	0.16	0.84	950	177.97
	63	200.00	200.00	12.00	8.00	88.00	88.00	0.00	0.00	0.00	305.00	305.00	31.45	0.16	0.84	950	186.27
	64	200.00	200.00	12.00	8.00	88.00	88.00	0.00	0.00	0.00	305.00	305.00	31.45	0.16	0.84	950	184.41
[47]	65	250.00	640.00	12.00	2.50	308.00	308.00	157.00	0.10	476.42	438.36	275.76	35.10	0.05	0.95	2400	899.16
	66	250.00	640.00	12.00	2.50	308.00	308.00	157.00	0.10	477.42	438.36	275.76	35.10	0.05	0.95	2400	911.04
	67	250.00	640.00	12.00	2.50	308.00	308.00	157.00	0.10	478.42	438.36	275.76	35.10	0.05	0.95	2400	887.64
	68	250.00	640.00	12.00	2.50	308.00	308.00	157.00	0.10	479.42	438.36	275.76	35.10	0.05	0.95	2400	886.08
[12]	69	250.00	400.00	8.00	10.00	192.00	192.00	401.92	0.40	479.42	400.00	420.00	61.90	0.08	0.38	1200	553.80
	70	250.00	400.00	8.00	10.00	192.00	192.00	401.92	0.40	479.42	400.00	420.00	82.30	0.08	0.38	1200	531.60
	71	250.00	400.00	8.00	10.00	192.00	192.00	401.92	0.40	479.42	400.00	420.00	61.90	0.08	0.47	1200	538.20
	72	250.00	400.00	8.00	10.00	192.00	192.00	200.96	0.20	479.42	400.00	420.00	61.90	0.08	0.92	1200	588.00
	73	120.00	400.00	6.00	6.00	194.00	194.00	401.92	0.84	479.42	400.00	420.00	61.90	0.08	0.42	1200	424.05
	74	150.00	500.00	6.00	8.00	244.00	244.00	401.92	0.54	479.42	400.00	420.00	61.90	0.08	0.37	1200	775.73
	75	180.00	600.00	6.00	10.00	294.00	294.00	401.92	0.37	479.42	400.00	420.00	61.90	0.07	0.33	1200	742.84
	76	210.00	700.00	6.00	12.00	344.00	344.00	401.92	0.27	479.42	400.00	420.00	61.90	0.07	0.30	1200	1680.69
	77	240.00	800.00	6.00	14.00	394.00	394.00	401.92	0.21	479.42	400.00	420.00	61.90	0.07	0.28	1200	2406.90
	78	120.00	600.00	8.00	6.00	292.00	292.00	401.92	0.56	479.42	400.00	420.00	61.90	0.08	0.34	1200	998.97
	79	150.00	700.00	8.00	8.00	342.00	342.00	401.92	0.38	479.42	400.00	420.00	61.90	0.07	0.30	1200	1515.84
	80	180.00	800.00	8.00	10.00	392.00	392.00	401.92	0.28	479.42	400.00	420.00	61.90	0.07	0.28	1200	1121.87
	81	210.00	400.00	8.00	12.00	192.00	192.00	401.92	0.48	479.42	400.00	420.00	61.90	0.09	0.47	1200	934.39

Appendix A - continuation

References	Number	x_1	x_2	x_3	x_4	x_5	x_6	x_7	x_8	x_9	x_{10}	x_{11}	x_{12}	x_{13}	x_{14}	x_{15}	Y
[12]	82	240.00	500.00	8.00	14.00	242.00	242.00	401.92	0.33	479.42	400.00	420.00	61.90	0.09	0.41	1200	1028.57
	83	120.00	700.00	10.00	6.00	340.00	340.00	401.92	0.48	479.42	400.00	420.00	61.90	0.08	0.32	1200	1456.93
	84	150.00	800.00	10.00	8.00	390.00	390.00	401.92	0.33	479.42	400.00	420.00	61.90	0.08	0.28	1200	1824.80
	85	180.00	400.00	10.00	10.00	190.00	190.00	401.92	0.56	479.42	400.00	420.00	61.90	0.10	0.44	1200	903.16
	86	210.00	500.00	10.00	12.00	240.00	240.00	401.92	0.38	479.42	400.00	420.00	61.90	0.09	0.39	1200	1127.33
	87	240.00	600.00	10.00	14.00	290.00	290.00	401.92	0.28	479.42	400.00	420.00	61.90	0.09	0.36	1200	1539.81
	88	120.00	800.00	12.00	6.00	388.00	388.00	401.92	0.42	479.42	400.00	420.00	61.90	0.08	0.31	1200	1963.41
	89	150.00	400.00	12.00	8.00	188.00	188.00	401.92	0.67	479.42	400.00	420.00	61.90	0.11	0.42	1200	915.76
	90	180.00	500.00	12.00	10.00	238.00	238.00	401.92	0.45	479.42	400.00	420.00	61.90	0.10	0.37	1200	1020.71
	91	210.00	600.00	12.00	12.00	288.00	288.00	401.92	0.32	479.42	400.00	420.00	61.90	0.09	0.34	1200	1540.81
	92	240.00	700.00	12.00	14.00	338.00	338.00	401.92	0.24	479.42	400.00	420.00	61.90	0.09	0.31	1200	1938.34
	93	120.00	500.00	14.00	6.00	236.00	236.00	401.92	0.67	479.42	400.00	420.00	61.90	0.10	0.37	1200	1176.83
	94	150.00	600.00	14.00	8.00	286.00	286.00	401.92	0.45	479.42	400.00	420.00	61.90	0.10	0.33	1200	1226.84
	95	180.00	700.00	14.00	10.00	336.00	336.00	401.92	0.32	479.42	400.00	420.00	61.90	0.09	0.30	1200	1720.04
	96	210.00	800.00	14.00	12.00	386.00	386.00	401.92	0.24	479.42	400.00	420.00	61.90	0.09	0.28	1200	2115.44
	97	240.00	400.00	14.00	14.00	186.00	186.00	401.92	0.42	479.42	400.00	420.00	61.90	0.12	0.50	1200	1338.63
[48]	98	640.00	250.00	14.00	2.50	306.00	306.00	307.72	0.19	437.72	640.13	372.45	32.39	0.12	0.88	1263	568.02
	99	640.00	250.00	12.00	2.50	308.00	308.00	307.72	0.19	437.72	640.13	372.45	56.54	0.11	0.89	1245	602.88
	100	640.00	250.00	12.00	2.50	308.00	308.00	904.32	0.57	459.54	640.13	372.45	32.39	0.11	0.89	1279	621.31
	101	640.00	200.00	12.00	2.50	308.00	308.00	307.72	0.24	437.72	640.13	372.45	32.39	0.13	0.87	1238	427.78
	102	640.00	250.00	12.00	2.50	308.00	308.00	307.72	0.19	437.72	640.13	372.45	32.39	0.11	0.89	1246	516.48
[49]	103	400.00	250.00	8.00	10.00	192.00	192.00	200.96	0.20	390.00	400.00	420.00	61.90	0.10	0.90	1250	581.25
	104	400.00	250.00	8.00	10.00	192.00	192.00	401.92	0.40	390.00	400.00	420.00	61.90	0.10	0.36	1250	553.75
	105	400.00	250.00	8.00	10.00	192.00	192.00	401.92	0.40	390.00	400.00	420.00	82.30	0.10	0.36	1250	560.63
	106	400.00	250.00	8.00	10.00	192.00	192.00	401.92	0.40	390.00	400.00	420.00	61.90	0.10	0.45	1250	587.50
	107	400.00	250.00	8.00	10.00	192.00	192.00	401.92	0.40	390.00	400.00	420.00	61.90	0.10	0.36	1250	609.38
[50]	108	200.00	150.00	4.00	4.00	96.00	96.00	0.00	0.00	0.00	295.00	295.00	54.40	0.10	0.90	640	80.40
	109	250.00	150.00	4.00	4.00	121.00	121.00	0.00	0.00	0.00	295.00	295.00	54.40	0.10	0.90	640	118.50
	110	300.00	150.00	4.00	4.00	146.00	146.00	0.00	0.00	0.00	295.00	295.00	54.40	0.10	0.90	640	173.50
	111	300.00	150.00	4.00	4.00	146.00	146.00	0.00	0.00	0.00	295.00	295.00	42.40	0.10	0.90	640	168.50
	112	300.00	150.00	4.00	4.00	146.00	146.00	0.00	0.00	0.00	295.00	295.00	61.30	0.10	0.90	640	176.50
	113	300.00	150.00	4.00	4.00	146.00	146.00	157.00	0.35	400.00	295.00	295.00	54.40	0.10	0.90	640	187.50
	114	300.00	150.00	4.00	4.00	146.00	146.00	157.00	0.35	400.00	295.00	295.00	54.40	0.10	0.90	640	182.50
	115	300.00	150.00	4.00	4.00	146.00	146.00	307.72	0.68	415.00	295.00	295.00	54.40	0.10	0.90	640	204.00
	116	300.00	150.00	4.00	4.00	146.00	146.00	508.68	1.13	418.00	295.00	295.00	54.40	0.10	0.90	640	216.50
[51]	117	250.00	400.00	8.00	10.00	192.00	192.00	803.84	0.80	390.00	400.00	420.00	60.00	0.08	0.41	1250	576.00
	118	250.00	400.00	8.00	10.00	192.00	192.00	803.84	0.80	390.00	400.00	420.00	80.00	0.08	0.41	1250	553.80
	119	250.00	400.00	8.00	10.00	192.00	192.00	803.84	0.80	390.00	400.00	420.00	60.00	0.08	0.49	1250	560.60
	120	250.00	400.00	8.00	10.00	192.00	192.00	803.84	0.80	390.00	400.00	420.00	60.00	0.08	0.41	1250	587.50
	121	250.00	400.00	8.00	10.00	192.00	192.00	803.84	0.80	390.00	400.00	420.00	60.00	0.08	0.41	1250	612.50
	122	250.00	400.00	8.00	10.00	192.00	192.00	803.84	0.80	390.00	400.00	420.00	60.00	0.08	0.33	1250	564.71

Appendix A - continuation

References	Number	x_1	x_2	x_3	x_4	x_5	x_6	x_7	x_8	x_9	x_{10}	x_{11}	x_{12}	x_{13}	x_{14}	x_{15}	y
[51]	123	250.00	400.00	8.00	10.00	192.00	192.00	803.84	0.80	390.00	400.00	420.00	60.00	0.08	0.58	1250	571.81
	124	250.00	400.00	8.00	10.00	192.00	192.00	803.84	0.80	390.00	400.00	420.00	60.00	0.08	0.66	1250	583.25
	125	250.00	400.00	8.00	10.00	192.00	192.00	803.84	0.80	390.00	400.00	420.00	40.00	0.08	0.41	1250	512.78
	126	250.00	400.00	8.00	10.00	192.00	192.00	803.84	0.80	390.00	400.00	420.00	50.00	0.08	0.41	1250	548.57
	127	250.00	400.00	8.00	10.00	192.00	192.00	803.84	0.80	390.00	400.00	420.00	70.00	0.08	0.41	1250	559.22
	128	250.00	400.00	8.00	10.00	192.00	192.00	803.84	0.80	390.00	270.00	282.00	80.00	0.08	0.41	1250	443.08
	129	250.00	400.00	8.00	10.00	192.00	192.00	803.84	0.80	390.00	448.00	468.00	80.00	0.08	0.41	1250	642.82
	130	250.00	400.00	8.00	10.00	192.00	192.00	803.84	0.80	390.00	483.00	504.00	80.00	0.08	0.41	1250	702.72
	131	250.00	400.00	8.00	10.00	192.00	192.00	803.84	0.80	390.00	529.00	552.00	80.00	0.08	0.41	1250	836.93
	132	250.00	400.00	8.00	6.00	192.00	192.00	803.84	0.80	390.00	400.00	420.00	60.00	0.06	0.42	1250	543.40
	133	250.00	400.00	8.00	8.00	192.00	192.00	803.84	0.80	390.00	400.00	420.00	60.00	0.07	0.42	1250	512.64
	134	250.00	400.00	8.00	12.00	192.00	192.00	803.84	0.80	390.00	400.00	420.00	60.00	0.09	0.40	1250	610.56
	135	250.00	400.00	8.00	14.00	192.00	192.00	803.84	0.80	390.00	400.00	420.00	60.00	0.09	0.39	1250	647.19
	136	250.00	400.00	6.00	10.00	192.00	192.00	803.84	0.80	390.00	400.00	420.00	60.00	0.07	0.42	1250	528.44
	137	250.00	400.00	7.00	10.00	192.00	192.00	803.84	0.80	390.00	400.00	420.00	60.00	0.07	0.41	1250	484.81
	138	250.00	400.00	9.00	10.00	192.00	192.00	803.84	0.80	390.00	400.00	420.00	60.00	0.08	0.40	1250	627.84
	139	250.00	400.00	10.00	10.00	192.00	192.00	803.84	0.80	390.00	400.00	420.00	60.00	0.09	0.40	1250	684.35
	140	250.00	360.00	8.00	10.00	192.00	192.00	803.84	0.89	390.00	400.00	420.00	60.00	0.09	0.34	1250	523.64
	141	250.00	380.00	8.00	10.00	192.00	192.00	803.84	0.85	390.00	400.00	420.00	60.00	0.08	0.38	1250	476.03
	142	250.00	420.00	8.00	10.00	192.00	192.00	803.84	0.77	390.00	400.00	420.00	60.00	0.07	0.44	1250	633.60
	143	250.00	440.00	8.00	10.00	192.00	192.00	803.84	0.73	390.00	400.00	420.00	60.00	0.07	0.46	1250	696.96
[52]	144	150.00	194.00	9.00	6.00	42.00	42.00	0.00	0.00	0.00	320.00	322.00	32.00	0.11	0.89	500	211.23
	145	150.00	194.00	9.00	6.00	42.00	42.00	0.00	0.00	0.00	320.00	322.00	46.90	0.11	0.89	500	220.88
	146	150.00	194.00	9.00	6.00	42.00	42.00	0.00	0.00	0.00	320.00	322.00	32.00	0.09	0.91	500	187.43
	147	150.00	194.00	9.00	6.00	42.00	42.00	0.00	0.00	0.00	320.00	322.00	32.00	0.08	0.92	500	192.12
	148	150.00	194.00	9.00	6.00	42.00	42.00	0.00	0.00	0.00	320.00	322.00	32.00	0.11	0.89	500	193.21
	149	150.00	194.00	9.00	6.00	37.00	37.00	0.00	0.00	0.00	320.00	322.00	32.00	0.11	0.89	500	160.36
	150	150.00	194.00	9.00	6.00	48.50	48.50	0.00	0.00	0.00	320.00	322.00	32.00	0.11	0.89	500	124.34
[53]	151	250.00	640.00	12.00	2.50	308.00	308.00	157.00	0.10	478.42	438.36	275.76	57.73	0.05	0.95	2400	1175.68
	152	200.00	640.00	12.00	2.50	308.00	308.00	157.00	0.12	478.42	438.36	275.76	35.10	0.05	0.95	2400	884.61

Appendix B

Number	All				Train (80 %)				Test (20 %)			
	min	max	mean	std	min	max	mean	std	min	max	mean	std
x_1	120.00	640.00	225.36	95.62	120.00	640.00	226.40	104.61	120.00	300.00	221.29	47.22
x_2	150.00	800.00	370.51	158.37	150.00	800.00	370.63	160.94	150.00	700.00	370.06	150.42
x_3	4.00	14.00	8.35	2.47	4.00	14.00	8.34	2.44	4.00	14.00	8.37	2.60
x_4	2.50	14.00	7.21	3.17	2.50	14.00	7.08	3.09	2.50	14.00	7.68	3.48
x_5	19.00	394.00	161.99	97.22	25.00	394.00	165.16	99.18	19.00	340.00	149.63	89.63
x_6	19.00	394.00	162.12	97.06	37.00	394.00	165.31	98.97	19.00	340.00	149.63	89.63
x_7	0.00	904.32	317.14	270.69	0.00	904.32	314.93	270.22	0.00	803.84	325.75	276.84
x_8	0.00	1.13	0.36	0.28	0.00	0.85	0.35	0.27	0.00	1.13	0.38	0.31
x_9	0.00	486.50	354.72	173.08	0.00	486.50	353.30	175.65	0.00	481.50	360.26	165.33
x_{10}	260.54	640.13	377.96	70.95	260.54	640.13	377.77	73.24	295.00	586.22	378.71	62.30
x_{11}	272.09	612.20	383.47	60.13	272.09	552.00	384.14	56.93	275.76	612.20	380.86	72.28
x_{12}	19.30	82.30	48.93	15.04	19.30	82.30	48.35	14.74	19.30	82.30	51.21	16.23
x_{13}	0.04	0.16	0.08	0.03	0.04	0.16	0.08	0.03	0.04	0.16	0.08	0.03
x_{14}	0.28	0.96	0.70	0.27	0.28	0.96	0.71	0.27	0.32	0.96	0.70	0.27
x_{15}	400.00	2,400.00	1,124.55	407.65	400.00	2,400.00	1,108.85	392.04	400.00	2,400.00	1,185.81	465.59
Y	64.87	2,406.90	529.36	461.70	64.87	2,406.90	532.36	476.71	85.02	1,539.81	517.67	404.66